

Deep Generative Endmember Modeling: An Application to Unsupervised Spectral Unmixing

Ricardo Augusto Borsoi, Tales Imbiriba, *Member, IEEE*, José Carlos Moreira Bermudez, *Senior Member, IEEE*

Abstract—Endmember (EM) spectral variability can greatly impact the performance of standard hyperspectral image analysis algorithms. Extended parametric models have been successfully applied to account for the EM spectral variability. However, these models still lack the compromise between flexibility and low-dimensional representation that is necessary to properly explore the fact that spectral variability is often confined to a low-dimensional manifold in real scenes. In this paper we propose to learn a spectral variability model directly from the observed data, instead of imposing it *a priori*. This is achieved through a deep generative EM model, which is estimated using a variational autoencoder (VAE). The encoder and decoder that compose the generative model are trained using pure pixel information extracted directly from the observed image, what allows for an unsupervised formulation. The proposed EM model is applied to the solution of a spectral unmixing problem, which we cast as an alternating nonlinear least-squares problem that is solved iteratively with respect to the abundances and to the low-dimensional representations of the EMs in the latent space of the deep generative model. Simulations using both synthetic and real data indicate that the proposed strategy can outperform the competing state-of-the-art algorithms.

Index Terms—Hyperspectral data, endmember variability, generative models, deep neural networks, variational autoencoders, spectral unmixing.

I. INTRODUCTION

Hyperspectral image analysis consists in a vast collection of algorithms and methods used to retrieve vital information from hyperspectral images (HI) in a increasing number of applications. Common applications include [1], [2] space exploration, remote sensing, surveillance, and, more recently, medical applications such as disease diagnosis and image-guided surgery [3]. One analysis methodology of particular interest is spectral unmixing (SU), which aims at retrieving sub-pixel information concerning the spectra of materials present in the scene, as well as estimating the proportions in which they contribute to each HI pixel.

Many parametric models have been proposed to describe the interaction between light and the target surface [4], [5]. The simplest of such models is the *Linear Mixing Model* (LMM), which considers that the observed reflectance of an HI pixel is obtained from a convex combination of the spectral signatures of pure materials. This model imposes a convex geometry to the SU problem, where all HI pixels are confined to a simplex

This work has been supported by the National Council for Scientific and Technological Development (CNPq).

R.A. Borsoi, T. Imbiriba and J.C.M. Bermudez are with the Department of Electrical Engineering, Federal University of Santa Catarina, Florianópolis, SC, Brazil. e-mail: raborsoi@gmail.com; talesim@gmail.com; j.bermudez@ieee.org.

Manuscript received Month day, year; revised Month day, year.

whose vertices are the pure material reflectances, usually termed endmembers (EMs). The linearity and convexity of the LMM model lead to an interpretation of its coefficients as the relative abundances of each pure material in the HI. Nevertheless, some characteristics of practical HIs cannot be modeled by the standard LMM, such as nonlinearities [5]–[8] or variations of the EMs along the image [9]–[11]. More sophisticated models are required when such nonidealities have important impact on the formation of the HI.

EM variability can originate from environmental conditions, illumination, or atmospheric or temporal changes [12]. Its occurrence may incur the propagation of significant estimation errors throughout the unmixing process [9]. Different strategies have been proposed to cope with EM variability in SU. They can be classified in methods that represent EMs as sets, methods that model EMs as statistical distributions, and methods that incorporate parametric representations of EM variability in the mixing model [13].

Parametric models are raising considerable interest since they lead to good unmixing results and avoid the main drawbacks of the other groups of SU methods that address EM variability, namely the dependence on *a priori* knowledge of libraries of material spectra or the need for strong assumptions on the statistical distribution of the EMs for mathematical tractability [12], [13]. Recently proposed parametric models attempt to capture spectral variability by extending the LMM using either additive [9] or multiplicative [10], [11], [14], [15] scaling factors, or by considering tensor-based formulations [16], [17]. Although SU methods based on extended parametric models offer different trade-offs between representation capacity and model complexity, they still fail to achieve a desirable balance between a low-dimensional representation and enough flexibility to represent complex EM variability. Specifically, they fail to properly explore the fact that, although being very complex and spectrally non-homogeneous, spectral variability in real scenes is often confined to low-dimensional manifolds [18]–[20]. Thus, existing models tend to be either too restrictive in their modeling capability or to lead to severely ill-posed estimation problems.

SU considering EM variability has also been formulated as a supervised learning problem, which is then solved without the need for an accurate physical model using neural networks (NNs) or support vector machines (SVMs) [21]–[24]. However, these strategies depend on the availability of vast amounts of training data to adequately capture the spectral diversity of real scenes. This makes the training process computationally intensive and often intractable for large EM libraries, which must also be known *a priori*. Some works attempt to reduce the

computational cost of these solutions by modifying learning algorithms to use hybrid soft-hard classification [25]–[27]. However, the resulting reconstructed abundance fractions do not have a clear physical interpretation due to the lack of a direct relationship to a physically motivated mixing model.

More recently, unsupervised SU approaches have also emerged by using autoencoders (AEC), which consist of encoder-decoder structured NNs originally devised for nonlinear dimensionality reduction [28]. These methods attempt to associate the decoder structure of the network with the LMM and the low-dimension representation of the input spectral vectors to the fractional abundances [29]. Different variations have been proposed, using pre-processing steps to reduce noise and outliers [30], [31], untangling the decoder from the encoder weights [32], using spectral angle distances to address nonlinear SU [33], or using denoising autoencoders to generate a robust initialization to matrix factorization-based SU strategies [34].

Despite their popularity, learning-based SU algorithms are still not able to properly address the spectral variability problem, as they depend on extremely high amounts of training data, leading to a computationally unfeasible learning process. Furthermore, the lack of a clear connection between AEC-based strategies and the physical mixing process makes one skeptical when concerning the robustness of AEC-based SU in face of more complex phenomena such as spectral variability.

In this work, we propose a novel SU formulation that leverages the advantages of deep learning methods to address EM variability while still maintaining a strong connection to the physical mixing process, and using limited amounts of training data. Specifically, we adopt a deep generative NN to represent the manifold of EM spectra, which is then incorporated within the LMM. Generative models such as variational autoencoders (VAE) [35] and generative adversarial networks (GAN) [36] have recently obtained excellent performance at learning the probability distribution of complex data sets in very high dimensional spaces (e.g. natural images) from relatively small amounts of training data. The structure of generative models allow one to find a low-dimensional latent representation that parsimoniously describes the variability of complex high-dimensional data sets. This leads to a low-dimensional parametrization of the training data distribution.

We formulate a novel unmixing strategy that can be cast as the problem of estimating the latent representations of the generative endmember models and the corresponding fractional abundances for each pixel in the HI. Specifically, we break down the SU problem in two steps. In the first step, we learn the latent EM variability manifold for each material in the scene using a deep generative EM model. The learning process uses pure pixel information directly extracted from the observed HI, which makes the proposed strategy suitable for unsupervised SU. In the second step, an alternating least-squares strategy is employed to estimate the parameters of an extended version of the LMM parametrized using the generative EM models obtained in the first step. The corresponding optimization problem is solved iteratively with respect to the abundances and to the low-dimensional representations of the EMs in the latent space of the deep

generative models.

As a result, the proposed approach benefits from the reduced dimension of the latent space. Moreover, unlike current approaches, the new method does not depend on the careful selection of regularization parameters to yield a good performance. The resulting algorithm is named *Deep Generative Unmixing algorithm* (DeepGU).

The proposed method is strongly related to parametric models and leverages the learning and generalization capability of deep neural networks to properly represent the manifold of EM variability. Hence, DeepGU leads to a model that is both low-dimensional and physically accurate, better describing the variability actually present in the scene.

Experimental results performed with both synthetic and real data indicate that the proposed strategy leads to more accurate abundance estimations than standard state-of-art SU methods accounting for EM variability. Qualitative analysis of the estimated abundance maps confirms these results. The improved accuracy comes at the expense of a small increase in the computational cost when compared to the best competing strategies.

This paper is organized as follows. Section II briefly reviews the LMM and its parametric extended versions. Section III discusses the basic properties of generative models in the context of VAE and GAN. Section IV introduces the proposed generative EM model and its learning strategy. In Section V we formulate the resulting SU problem, present the DeepGU algorithm, and discuss aspects of the proposed optimization strategy. The neural network architecture is discussed in Section VI. The performance of the proposed method is compared with that of competing algorithms in Section VII. Finally, the conclusions are presented in Section VIII.

II. LINEAR MIXING MODELS

The Linear Mixing Model (LMM) [4] assumes that a given n -th pixel $\mathbf{y}_n \in \mathbb{R}^L$, with L bands, is represented as

$$\mathbf{y}_n = \mathbf{M}\mathbf{a}_n + \mathbf{e}_n, \quad \text{subject to } \mathbf{1}^\top \mathbf{a}_n = 1 \text{ and } \mathbf{a}_n \geq \mathbf{0} \quad (1)$$

where $\mathbf{M} \in \mathbb{R}^{L \times P}$ is a matrix whose columns are the P EM spectral signatures \mathbf{m}_k , \mathbf{a}_n is the abundance vector and \mathbf{e}_n is an additive white Gaussian noise (WGN). The LMM assumes that the EM spectra are fixed for all HI pixels \mathbf{y}_n , $n = 1, \dots, N$. This assumption jeopardizes the accuracy of estimated abundances in many circumstances due to the spectral variability existing in a typical scene.

Different parametric models have been recently proposed to account for variable EM spectra within a given scene [9]–[11]. These models can be generically described as

$$\mathbf{y}_n = f(\mathbf{M}_0, \boldsymbol{\theta}_n)\mathbf{a}_n + \mathbf{e}_n \quad (2)$$

where f is a parametric function, $\mathbf{M}_0 \in \mathbb{R}^{L \times P}$ is a reference EM matrix, and $\boldsymbol{\theta}_n$ is a vector of parameters describing the manifold of EM variability.

Different functional forms have been proposed for $f(\mathbf{M}_0, \boldsymbol{\theta}_n)$ to account for EM variability in this framework, such as additive [9] or multiplicative [10], [11] variability factors acting upon the reference EM matrix \mathbf{M}_0 . However,

these models fail to achieve a desirable balance between a low-dimensional representation and enough flexibility to represent complex variability patterns. They tend to be either too restrictive in their modeling capability, or to lead to ill-posed optimization problems. Instead of using a pre-defined parametric model, we propose to address this issue by learning a parametric function $f(\mathbf{M}_0, \theta_n)$ using a generative model.

III. GENERATIVE MODELS

Generative models attempt to estimate the probability distribution $p(X)$ of a random variable $X \in \mathbb{R}^L$ based on a set of observations $\mathbf{x}_i, i = 1, \dots, N_x$ in such a way that allows one to generate new samples that look similar to new realizations of X . The main characteristic of this problem, which sets it apart of other unsupervised learning methods such as density estimation, is the fact that we must to be able to sample from the estimated model $\hat{p}(X)$.

In many practical applications of interest, the dimensionality L of the variable of interest X is very high. This makes the general problem very difficult, as it amounts to estimating and sampling from an arbitrary high-dimensional probability density function [37], [38]. Nonetheless, the distributions of interest are often supported at a low-dimensional manifold of a set of so-called latent variables, and this fact can be explored to make the problem more tractable. A convenient way to address this problem is to define a new random variable $\mathbb{R}^K \ni Z \sim p(Z)$ with a known distribution in a low-dimensional space (e.g. an isotropic Gaussian distribution with $K \ll L$), and a parametric function (e.g. a neural network) \mathcal{G}_θ mapping $Z \mapsto \hat{X} \in \mathbb{R}^L$ such that the image of Z by \mathcal{G}_θ is a random variable whose distribution is very close to $p(X)$. In other words, the goal becomes to learn the parameters θ of \mathcal{G}_θ such that the distribution of $\hat{X} = \mathcal{G}_\theta(Z)$ is as close to $p(X)$ as possible. Then, samples of \hat{X} can be generated by sampling from $Z \sim p(Z)$ and using the mapping $\mathcal{G}_\theta(Z)$.

Although estimating θ may still seem difficult at first, recent advances in machine learning such as VAEs [35] and GANs [36] have shown formidable performance at learning complex distributions such as those of natural images.

VAEs address this problem by assuming that the distribution of the observed data X follows a directed graphical model $p(X|Z)$, which is represented by the function \mathcal{G}_θ . The parameters of \mathcal{G}_θ are learned by minimizing a lower bound on the log-likelihood of $p(X)$ [35]:

$$\log p(X) \geq \mathbb{E}_{q_\phi(Z|X)} \{ \log p(X|Z) \} - KL(q_\phi(Z|X) \| p(Z)) \quad (3)$$

where $KL(\cdot \| \cdot)$ is the Kullback-Leibler divergence between two distributions, $\mathbb{E}_\varsigma \{ \cdot \}$ is the expected value operator with respect to the distribution ς and $q_\phi(Z|X)$ is a variational approximation to the intractable posterior $p(Z|X)$, which is modeled by a function \mathcal{D}_ϕ (e.g. another neural network) parameterized in ϕ . Note that $q_\phi(Z|X)$ must be a high-capacity distribution¹, so that it can provide a good approximation of

¹Capacity of a distribution is a generic term to describe how complex a relationship it can model.

the posterior $p(Z|X)$, which then allows the lower bound in (3) to be close to the true value of $\log p(X)$ [39].

GANs, on the other hand, attempt to learn the distribution $p(X)$ by searching for the Nash equilibrium of a two-player adversarial game [36]. A generator network \mathcal{G}_θ tries map the distribution of the latent variables Z into the data distribution of X , and a discriminator network \mathcal{C}_ϕ tries to predict the probability of a random sample \mathbf{x}_i coming from the true distribution $p(X)$ instead of being generated through \mathcal{G}_θ . The generator \mathcal{G}_θ is trained by maximizing the probability of the discriminator making a mistake. This is formulated as the minimax optimization problem

$$\begin{aligned} \min_{\mathcal{G}_\theta} \max_{\mathcal{C}_\phi} & \mathbb{E}_{p(X)} \{ \log \mathcal{C}_\phi(X) \} \\ & + \mathbb{E}_{p(Z)} \{ (1 - \mathcal{C}_\phi(\mathcal{G}_\theta(Z))) \}. \end{aligned} \quad (4)$$

GANs are more flexible and have shown better performance at approximating complex distributions such as natural images (leading to sharper results) when compared to VAEs [36]. However, GANs are also much harder to train [38]. Moreover, VAEs naturally offer a way to obtain the latent representations of corresponding to samples $\mathbf{x}_i \sim p(X)$ by mapping $X \mapsto Z$ using the function \mathcal{D}_ϕ , which is also called an encoder model. This property and their stable training have motivated us to use VAEs in this work.

IV. A DEEP GENERATIVE ENDMEMBER MODEL

In this section, we propose to model the distribution of EM spectral variability using a deep generative model. By doing so, we can explicitly explore a common property of spectral variability: the EM spectra are usually confined to a low-dimensional manifold. This property is due to the fact that the spectral signature of many materials is a function of a few photometric or chemical properties of the medium. Prominent examples include packed particle spectra as a function of its roughness, size and density [18], leaf reflectance spectra as a function of various biophysical parameters [19], and soil reflectance as a function of moisture conditions [20].

A. The steps of the proposed SU method

We assume the existence of nonlinear functions \mathcal{G}_{θ_p} , $p = 1, \dots, P$ (the generative model) that map latent representations \mathbf{z}_p into their corresponding spectral signatures \mathbf{m}_p . We assume also the existence of encoder models \mathcal{D}_{ϕ_p} that map spectral signatures into their latent representations. In other words, we assume that any arbitrary observation \mathbf{m}_p of a spectral signature of a material belongs to the set

$$\mathbf{m}_p \in \{ \mathcal{G}_{\theta_p}(\mathbf{z}_p) : \mathbf{z}_p \in \mathbb{R}^K \} \quad (5)$$

and thus can be equivalently represented by a corresponding low-dimensional vector $\mathbf{z}_p \in \mathbb{R}^K$ in the latent space of the generative model \mathcal{G}_{θ_p} . This reasoning is illustrated in Fig. 1, where the encoder function \mathcal{D}_ϕ maps the input EM signature to the low-dimensional manifold. Reciprocally, low-dimensional vectors in the latent space can be mapped (decoded) to their corresponding spectral signatures using \mathcal{G}_θ .

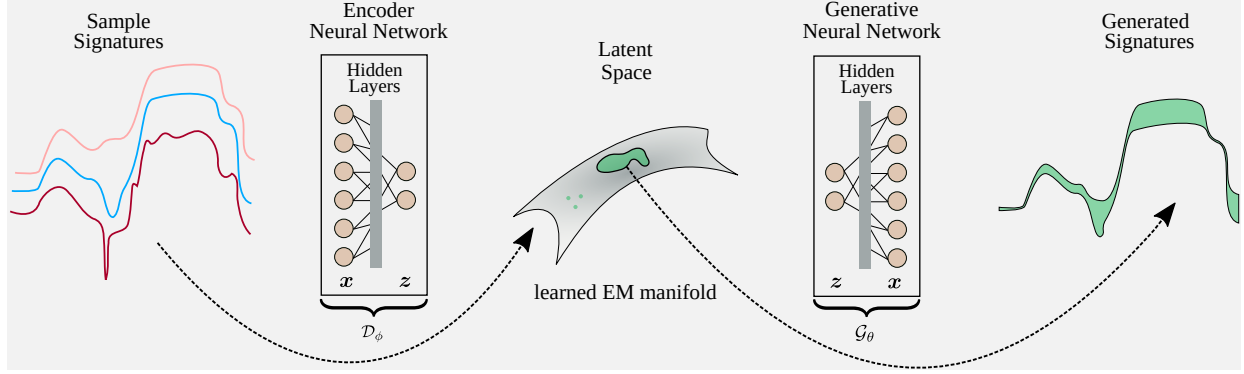


Figure 1: Illustration of the proposed Deep Generative Endmember Model.

As such, we can formulate EM estimation in the SU problem in the latent domain (as opposed to the input spectral space), which is of a much lower order. Moreover, this approach will keep the physical interpretation of the model, provided that we have relevant training data to learn the generative models [40]–[43]. This strategy relies on the existence of a priori training data for each material in the image, which might come in the form of, e.g., spectral libraries of laboratory measurements [44]. Nevertheless, we propose a more practical and effective approach to train the generators \mathcal{G}_{θ_p} by exploring information contained in multiple pure pixels extracted from the observed HI. The presence of multiple pure pixels in an observed HI is a characteristic of many real scenes, and can be leveraged to help in estimating the EM models, thus, reducing the ill-posedness of the SU problem².

Therefore, we propose to break the unmixing problem into a sequence of two problems:

- Using pure pixel information extracted from the HI by standard EM extraction methods, learn the generative and encoder models, \mathcal{G}_{θ_p} and \mathcal{D}_{ϕ_p} , for all EMs in the scene ($p = 1, \dots, P$).
- Using the learned generative models, solve the SU problem by estimating the latent EM representations $\mathbf{Z}_n = [z_{1,n}, \dots, z_{P,n}]$ and the fractional abundance vectors \mathbf{a}_n that can best represent the observed hyperspectral data, for all pixels in the scene ($n = 1, \dots, N$).

B. Learning the generative and encoder models \mathcal{G}_{θ_p} and \mathcal{D}_{ϕ_p}

The objective of this first problem is to estimate the generative and encoding models \mathcal{G}_{θ_p} and \mathcal{D}_{ϕ_p} , for $p = 1, \dots, P$. We assume the knowledge of a set $\mathcal{N}_{P,p}$ of pure pixels for the p -th EM, for all $p = 1, \dots, P$. Multiple pure pixels exist in many scenes, and can be directly extracted from the observed HI using automated EM extraction techniques [45], [46]. The sets of pure pixels $\mathcal{N}_{P,p}$, which can be seen as observations from the statistical distribution of each EM, are then used in the form of training data to learn the models \mathcal{G}_{θ_p} and \mathcal{D}_{ϕ_p} using a VAE [35]. If the set $\mathcal{N}_{P,p}$ is representative of the variability of the p -th material, the learned generative model

²Pure pixels are defined here as a set of pixels whose spectral distance relative to the reference EMs in \mathbf{M}_0 is less than a specified threshold.

\mathcal{G}_{θ_p} will be able to accurately describe the manifold of the p -th EM variability. Doing the same for all $p = 1, \dots, P$ yields a set of variability models for all the EM spectra.

Although the extraction of multiple pure pixels from observed HIs is a well-established technique used to produce EM libraries [45], mixed pixels can sometimes be mistakenly identified as a pure pixel of some of the EMs. This constitutes a problem for library-based SU applications (e.g. MESMA and sparse SU) since some of the library spectra may end up not being representative of their EM class (material).

The smooth nature of the latent representation of VAEs allows the mitigation of this problem in the proposed approach. Assuming the availability of a reference EM matrix \mathbf{M}_0 of correctly identified signatures (which can be obtained using any EM extraction method) and of a set of encoder models \mathcal{D}_{ϕ_p} , we can compute the latent representation of these reference signatures of each EM as

$$\begin{aligned} \mathbf{Z}_0 &= [z_{1,0}, \dots, z_{P,0}] \\ &= [\mathcal{D}_{\phi_1}(\mathbf{m}_{1,0}), \dots, \mathcal{D}_{\phi_P}(\mathbf{m}_{P,0})]. \end{aligned} \quad (6)$$

where $\mathbf{m}_{p,0}$ is the p -th column of \mathbf{M}_0 . The latent representation $z_{p,0}$ can be used as a reference latent code for the p -th material. Thus, we can evaluate whether an estimated EM latent representation corresponds to a pure pixel z_p associated with a reference latent representation $z_{p,0}$ by testing if it is sufficiently close to $z_{p,0}$. This can be performed since the output of VAEs have been shown to vary smoothly with changes of the latent variable [35]. Thus, we can use \mathbf{Z}_0 to regularize the SU problem to prevent $\mathcal{G}_{\theta_p}(z_p)$ from representing mixed pixels. This increases the robustness of the proposed approach.

V. THE UNMIXING ALGORITHM

Given a set of generative models $\mathcal{G}_{\theta_p} : \mathbb{R}^K \rightarrow \mathbb{R}^L$, $p = 1, \dots, P$ for each EM in the scene, a latent space representation \mathbf{Z}_0 of a reference EM matrix \mathbf{M}_0 , and an HI $\mathbf{Y} = [\mathbf{y}_1, \dots, \mathbf{y}_N]$, the SU problem can be cast as the minimization of a risk functional of the form

$$J(\mathbf{A}, \mathbf{Z}) = \frac{1}{2} \sum_{n=1}^N \|\mathbf{y}_n - \tilde{\mathcal{G}}(\mathbf{Z}_n) \mathbf{a}_n\|_F^2 + \mathcal{R}(\mathbf{A}) + \mathcal{R}(\mathbf{Z}) \quad (7)$$

where $\mathbf{A} = [\mathbf{a}_1, \dots, \mathbf{a}_N] \in \mathbb{R}^{P \times N}$ is the abundance matrix, $\mathbb{Z} \in \mathbb{R}^{N \times P \times K}$ is a 3-D tensor obtained by stacking all pixel-dependent latent EM representations \mathbf{Z}_n , such that $[\mathbb{Z}]_{n,:,:} = \mathbf{Z}_n$, $\mathcal{R}(\mathbf{A})$ and $\mathcal{R}(\mathbb{Z})$ are regularization terms to improve the problem conditioning, and the matrix-valued function $\tilde{\mathcal{G}}(\mathbf{Z}_n)$ defined as

$$\tilde{\mathcal{G}}(\mathbf{Z}_n) = [\mathcal{G}_{\theta_1}(\mathbf{z}_{1,n}), \dots, \mathcal{G}_{\theta_P}(\mathbf{z}_{P,n})], \quad n = 1, \dots, N$$

is the concatenation of the generative functions for each EM.

The term $\mathcal{R}(\mathbf{A})$ is a regularization functional that aims to provide spatial smoothness and to enforce positivity and sum-to-one constraints to the abundances. It is given by [11]

$$\mathcal{R}(\mathbf{A}) = \lambda_A (\|\mathcal{H}_h(\mathbf{A})\|_{2,1} + \|\mathcal{H}_v(\mathbf{A})\|_{2,1}) + \iota_{\mathcal{S}^1}(\mathbf{A}) \quad (8)$$

where parameter λ_A controls the contribution of this term to the cost function. The first two terms are a spatial regularizers over \mathbf{A} , where \mathcal{H}_h and \mathcal{H}_v are linear operators that compute the first-order horizontal and vertical gradients of a bidimensional signal, acting separately for each material of \mathbf{A} , and $\|\cdot\|_{2,1}$ is the $\mathcal{L}_{2,1}$ norm, defined as $\|\mathbf{X}\|_{2,1} = \sum_{n=1}^N \|\mathbf{x}_n\|_2$. The term $\iota_{\mathcal{S}^1}(\mathbf{A})$ is the indicator function of the unity simplex, i.e. $\iota_{\mathcal{S}^1}(\mathbf{A}) = 0$ if $\mathbf{A} \in \mathcal{S}^1$ and $\iota_{\mathcal{S}^1}(\mathbf{A}) = \infty$ otherwise, where

$$\mathcal{S}^1 = \{\mathbf{A} \in \mathbb{R}^{P \times N} : \mathbf{A} \geq 0, \mathbf{1}^\top \mathbf{A} = \mathbf{1}^\top\}. \quad (9)$$

The term $\mathcal{R}(\mathbb{Z})$ constrains the EM latent representations \mathbb{Z} to be close to the latent representation \mathbf{Z}_0 of the reference EM matrix \mathbf{M}_0 . It is given by

$$\mathcal{R}(\mathbb{Z}) = \frac{\lambda_Z}{2} \sum_{n=1}^N \|\mathbf{Z}_n - \mathbf{Z}_0\|_F^2 \quad (10)$$

where parameter λ_Z controls the contribution of this term to the cost function. This regularization makes the estimation problem more robust to the selection of the training data $\mathcal{N}_{\mathcal{P},p}$ by assuring the closeness of the estimated latent codes \mathbb{Z} and the representations of pure pixels of each class.

The optimization problem then becomes

$$(\hat{\mathbf{A}}, \hat{\mathbb{Z}}) = \arg \min_{\mathbf{A}, \mathbb{Z}} J(\mathbf{A}, \mathbb{Z}). \quad (11)$$

The problem defined in (11) is non-smooth and non-convex with respect to both variables \mathbf{A} , and \mathbb{Z} . However, we can find a local stationary point by minimizing (11) iteratively with respect to each variable, leading to the Deep Generative Unmixing (DeepGU) method described in Algorithm 1. We next describe the details of each optimization step. Implementation details are described in Sections VI and VII.

A. Optimization with respect to \mathbb{Z}

Rewriting (11) considering only the terms in (7) that depend on \mathbb{Z} , the problem becomes

$$\min_{\mathbb{Z}} \frac{1}{2} \sum_{n=1}^N \left(\|\mathbf{y}_n - \tilde{\mathcal{G}}(\mathbf{Z}_n) \mathbf{a}_n\|_F^2 + \lambda_Z \|\mathbf{Z}_n - \mathbf{Z}_0\|_F^2 \right) \quad (12)$$

This is a regularized nonlinear least squares problem, which can be solved individually for each pixel \mathbf{y}_n . Thus, (12) can be decomposed into N non-convex, nonlinear optimization

Algorithm 1: DeepGU algorithm for solving (11)

Input : \mathbf{Y} , λ_Z , and λ_A .
Output: $\hat{\mathbf{A}}$ and $\hat{\mathbb{Z}}$.

- 1 Estimate the reference EM signatures \mathbf{M}_0 using an EM extraction method;
- 2 Estimate $\mathbf{A}^{(0)}$ using a standard LMM-based SU method;
- 3 Extract sets of pure pixels $\mathcal{N}_{\mathcal{P},p}$, $p = 1, \dots, P$ from the HI using a bundle extraction strategy;
- 4 Train the generative and encoder models \mathcal{G}_{θ_p} , \mathcal{D}_{ϕ_p} , $p = 1, \dots, P$;
- 5 Compute the latent representation of \mathbf{M}_0 as $\mathbf{Z}_0 = [\mathcal{D}_{\phi_1}(\mathbf{m}_{1,0}), \dots, \mathcal{D}_{\phi_P}(\mathbf{m}_{P,0})]$;
- 6 Set $i = 0$;
- 7 **while** stopping criterion is not satisfied **do**
- 8 $i = i + 1$;
- 9 $\mathbb{Z}^{(i)} = \arg \min_{\mathbb{Z}} J(\mathbf{A}^{(i-1)}, \mathbb{Z})$;
- 10 $\mathbf{A}^{(i)} = \arg \min_{\mathbf{A}} J(\mathbf{A}, \mathbb{Z}^{(i)})$;
- 11 **end**
- 12 **for** $n = 1, \dots, N$, **do**, $[\hat{\mathbb{Z}}]_{:, :, n} = \tilde{\mathcal{G}}([\mathbb{Z}]_{:, :, n})$, **end**;
- 13 **return** $\hat{\mathbf{A}} = \mathbf{A}^{(i)}$, $\hat{\mathbb{Z}}$;

problems with dimensionality $K \times P$. We solve each of those problems using a quasi-Newton algorithm, described in Algorithm 2, which provides an efficient solution for high-dimensional functions $\tilde{\mathcal{G}}$ [47]. Although problem (12) is generally non-convex, recent research [48] has proven that, under suitable assumptions on the generator network $\tilde{\mathcal{G}}$, the problem of recovering the latent variable \mathbf{Z}_n does not have any stationary point (e.g. local minima or saddle points) outside a small neighborhood of the desired solution and its negative scalar multiple. This indicates the existence of a favorable global geometry of (12).

Note that $\tilde{\mathcal{G}}$ is not necessarily a differentiable function, which can make the optimization problem more challenging. Nonetheless, quasi-Newton algorithms show excellent performance at non-smooth problems [49], where convergence is generally observed as long as the line search procedure does not return a point at which the objective function is non-differentiable. While quasi-Newton algorithms can be directly applied to obtain approximate solutions to non-smooth problems [49], [50], specialized methodologies with global convergence guarantees can be employed (at the cost of an increased computational complexity) if a precise solution is necessary [50]. We shall restrict ourselves to the quasi-Newton method for computational efficiency.

B. Optimization with respect to \mathbf{A}

Restating (11) considering only the terms in (7) that depend on \mathbf{A} leads to

$$\min_{\mathbf{A}} \frac{1}{2} \sum_{n=1}^N \|\mathbf{y}_n - \tilde{\mathcal{G}}(\mathbf{Z}_n) \mathbf{a}_n\|_F^2 + \iota_{\mathcal{S}^1}(\mathbf{A}) \quad (13)$$

$$+ \lambda_A (\|\mathcal{H}_h(\mathbf{A})\|_{2,1}^2 + \|\mathcal{H}_v(\mathbf{A})\|_{2,1}^2).$$

Algorithm 2: Quasi-Newton algorithm for solving (12)

Input : \mathbf{a}_n , \mathbf{y}_n , λ_Z , \mathbf{Z}_0 , \mathbf{z}_0 and J .
Output: \mathbf{Z}_n .
1 Set $i = 0$ and $\mathbf{B}_1 = \mathbf{I}$;
2 **while** stopping criterion is not satisfied **do**
3 $i = i + 1$;
4 Compute search direction $\mathbf{p}_i = -\mathbf{B}_i \nabla J_k$;
5 Set $\mathbf{z}_{i+1} = \mu_i \mathbf{p}_i$, where μ_i is computed using a line search procedure to satisfy the Wolfe conditions;
6 Define $\mathbf{s}_i = \mathbf{z}_{i+1} - \mathbf{z}_i$ and $\mathbf{u}_i = \nabla J_{i+1} - \nabla J_k$;
7 $\mathbf{B}_{i+1} = \mathbf{B}_i - \frac{\mathbf{B}_i \mathbf{s}_i \mathbf{s}_i^\top \mathbf{B}_i}{\mathbf{s}_i^\top \mathbf{B}_i \mathbf{s}_i} + \frac{\mathbf{u}_i \mathbf{u}_i^\top}{\mathbf{u}_i^\top \mathbf{s}_i}$;
8 **end**
9 Reorder \mathbf{z}_{i+1} as a matrix \mathbf{Z}_n ;
10 **return** $\widehat{\mathbf{Z}}_n = \mathbf{Z}_n$;

Table I: Encoder network architecture.

Layer	Activation Function	Number of units
Input	—	L
Hidden # 1	ReLU	$\lceil 1.2 \times L \rceil + 5$
Hidden # 2	ReLU	$\max \{ \lceil L/4 \rceil, K+2 \} + 3$
Hidden # 3	ReLU	$\max \{ \lceil L/10 \rceil, K+1 \}$

Since the latent variables \mathbf{Z}_n are fixed, (13) consists of a SU problem with a pixel-dependent EM matrix and an edge-preserving spatial regularization. Although this problem is not separable with respect to each pixel in the image, the Alternating Direction Method of the Multipliers (ADMM) can be used to obtain an efficient solution [51]. The solution of (13) using the ADMM is well described elsewhere (e.g. [10]) and will thus be omitted here for conciseness.

VI. NEURAL NETWORK ARCHITECTURE

As discussed before, we used a VAE [35] to learn the generative and encoder models \mathcal{G}_{θ_p} and \mathcal{D}_{ϕ_p} from the sets of pure pixels $\mathcal{N}_{\mathcal{P},p}$. Compared to GANs, the training of VAEs is much simpler and more stable [38]. Moreover, VAEs naturally return the encoder model \mathcal{D}_{ϕ_p} as an approximation to the posterior distribution when learning \mathcal{G}_{θ_p} . We have selected a dimension $K = 2$ for the latent space, as it was experimentally verified to be sufficient to adequately capture the variability of each single material in a scene.

For the network architectures, we selected the number of layers and neurons according to the autoencoder implementation in [28], [52], with three hidden layers using ReLU activations (defined as $\text{ReLU}(x) = \max(x, 0)$) in the hidden layers, which are described in more detail in Tables I and II.

We found that this configuration led to spectrally smooth generated signatures, and was effective at generalizing well with small training sample sizes. We trained the network for 50 epochs with the Adam optimizer [53] in TensorFlow, using a batch optimization with mini-batch size equal to one third of the total amount of training data for each EM.

Table II: Decoder network architecture.

Layer	Activation Function	Number of units
Hidden # 1	ReLU	$\max \{ \lceil L/10 \rceil, K+1 \}$
Hidden # 2	ReLU	$\max \{ \lceil L/4 \rceil, K+2 \} + 3$
Hidden # 3	ReLU	$\lceil 1.2 \times L \rceil + 5$
Output	Sigmoid	L

Table III: Simulation results using synthetic data.

Data Cube 1 – DC1					
	RMSE _A	RMSE _M	SAM _M	RMSE _Y	Time [s]
FCLS	0.1161	—	—	0.0253	0.71
PLMM	0.1059	0.0787	0.0440	0.0005	122.09
ELMM	0.1039	0.0756	0.0398	0.0232	8.82
GLMM	0.1009	0.0759	0.0355	0.0169	23.74
DeepGU	0.0230	0.0692	0.0233	0.0323	75.20
Data Cube 2 – DC2					
	RMSE _A	RMSE _M	SAM _M	RMSE _Y	Time [s]
FCLS	0.0591	—	—	0.0255	0.38
PLMM	0.0547	0.0297	0.0378	0.0218	41.31
ELMM	0.0507	0.0349	0.0382	0.0149	20.25
GLMM	0.0523	0.0329	0.0367	0.0147	17.03
DeepGU	0.0442	0.0286	0.0323	0.0249	36.40

VII. EXPERIMENTAL RESULTS

In this section, simulation results using both synthetic and real data illustrate the performance of the proposed method. We compare the proposed DeepGU method with the fully constrained least squares (FCLS), the PLMM [9], the ELMM [10], and the GLMM [11]. In all experiments, the VCA algorithm [54] was used to extract the reference EM matrix \mathbf{M}_0 from the observed HI and to initialize the different methods. The abundance maps were initialized using the results obtained by the FCLS algorithm. The sets $\mathcal{N}_{\mathcal{P},p}$ of pure pixels were constructed by selecting the image pixels \mathbf{y}_n with the smallest spectral angle relative to the reference EMs in \mathbf{M}_0 . We run the alternating optimization process in Algorithm 1 for at most 10 iterations or until the relative change of \mathbf{A} and \mathbb{Z} was less than 10^{-3} . The iterative procedure in Algorithm 2 is run until the relative change of \mathbf{z}_i is less than 10^{-3} . The performances were evaluated using the Root Means Squared Error (RMSE) between the estimated abundance maps (RMSE_A), between the EM matrices (RMSE_M) and between the reconstructed images (RMSE_Y). The RMSE between two generic tensors is defined as

$$\text{RMSE}_{\mathbb{X}} = \sqrt{\frac{1}{N_{\mathbb{X}}} \|\mathbb{X} - \mathbb{X}^* \|_F^2} \quad (14)$$

where $N_{\mathbb{X}}$ denotes the number of elements in the tensor \mathbb{X} .

We consider also the Spectral Angle Mapper (SAM) to evaluate the estimated EMs

$$\text{SAM}_{\mathbb{M}} = \frac{1}{N} \sum_{n=1}^N \sum_{p=1}^P \arccos \left(\frac{\mathbf{m}_{p,n}^\top \mathbf{m}_{p,n}^*}{\|\mathbf{m}_{p,n}\| \|\mathbf{m}_{p,n}^*\|} \right). \quad (15)$$

A. Synthetic data

To quantitatively compare the different algorithms, two synthetic datasets were created, namely Data Cube 1 (DC1)

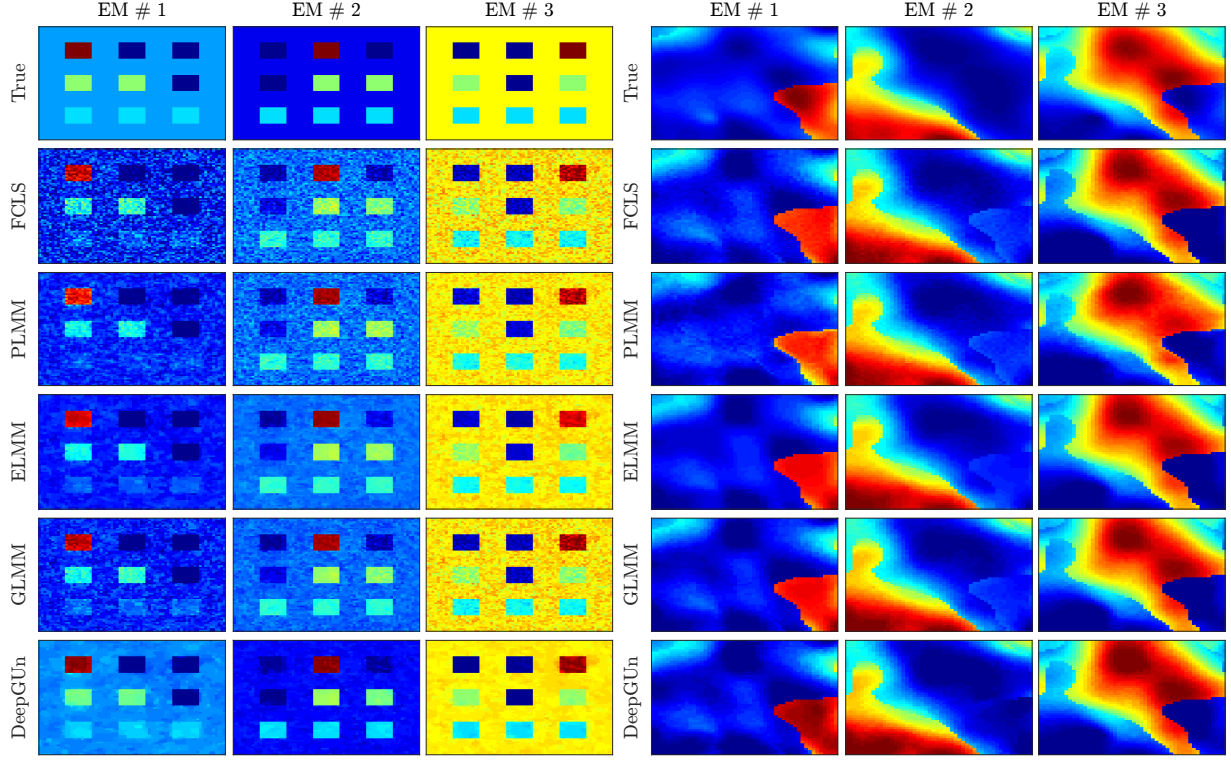


Figure 2: Abundance maps of (left–right) DC1 and DC2 for all tested algorithms. Abundance values represented by colors ranging from blue ($\alpha_k = 0$) to red ($\alpha_k = 1$).

and Data Cube 2 (DC2), with 70×70 pixels (DC1) and 50×50 pixels (DC2). These datasets were built using three 224-band EMs extracted from the USGS Spectral Library [55] and spatially correlated abundance maps, as depicted in the first row of Fig. 2.

Spectral variability of the EMs was imposed using two different models. For the DC1 datacube, we adopted the variability model used in [9], consisting of pixelwise multiplicative spectral factors given by random piecewise-linear functions. For DC2, the variability model of [11] was used, consisting of band dependent scaling factors that varied smoothly in both the spatial and spectral dimensions. White Gaussian noise was finally added to all datasets to yield a 30dB SNR.

The optimal parameters for each algorithm were selected by performing grid searches for each dataset. The ranges in which the parameters were searched were selected according to those discussed by the authors in the original publications. For the PLMM we searched for α , β and γ in the ranges $[0.01, 0.1, 0.35, 0.7, 1.4, 25]$, $[10^{-9}, 10^{-5}, 10^{-4}, 10^{-3}]$ and $[10^{-2}, 0.1, 1, 10, 10^2]$, respectively. For both ELMM and GLMM, the parameters were selected among the following values: $\lambda_S, \lambda_M \in [0.01, 0.1, 1, 5, 10, 50]$, $\lambda_A \in [0.001, 0.01, 0.05]$, and $\lambda_\psi, \lambda_\Psi \in [10^{-6}, 10^{-3}, 1, 10^3]$. For the proposed DeepGU algorithm, we fixed $\lambda_Z = 0.1$ and selected λ_A among the values $[0.005, 0.01, 0.05]$. For the proposed method, the sets of pure pixels for each EM $\mathcal{N}_{P,p}$ were constructed by selecting the 100 pixels closest to the reference materials M_0 .

The quantitative results are shown in Table III, with the best results for each metric marked in bold. The proposed method

clearly outperformed the competing algorithms in terms of RMSE_A for both datasets. Qualitatively, the abundance maps provided by DeepGU, displayed in Fig. 2, are clearly much closer to the true abundance maps than those provided by the other methods. These are important results, as accuracy in abundance estimation is the main objective of SU.

For the EM reconstruction metrics RMSE_M and SAM_M , DeepGU gave the best results for both data cubes. This indicates that the proposed endmember model used by DeepGU allows for precise material identification from the observed hyperspectral scenes.

The reconstruction error RMSE_Y of the DeepGU algorithm was comparable to the FCLS and significantly larger than that of the GLMM. This is natural since the GLMM has more degrees of freedom. However, the connection between RMSE_Y and the abundance reconstruction error is far from being direct, as can be seen in Table III.

The execution times, at the rightmost column of Table III, indicate that the computational complexity of DeepGU is somewhere between the complexities of GLMM and PLMM, the two major competing algorithms. Hence, the DeepGU method yielded superior SU performance, with easier parameter tuning, and at a reasonable computational cost.

B. Real data

We considered the Cuprite and Houston datasets for the simulations with real data. These datasets, originally discussed in [10], were captured by the AVIRIS instrument and had 224 bands. The spectral bands corresponding to water absorption

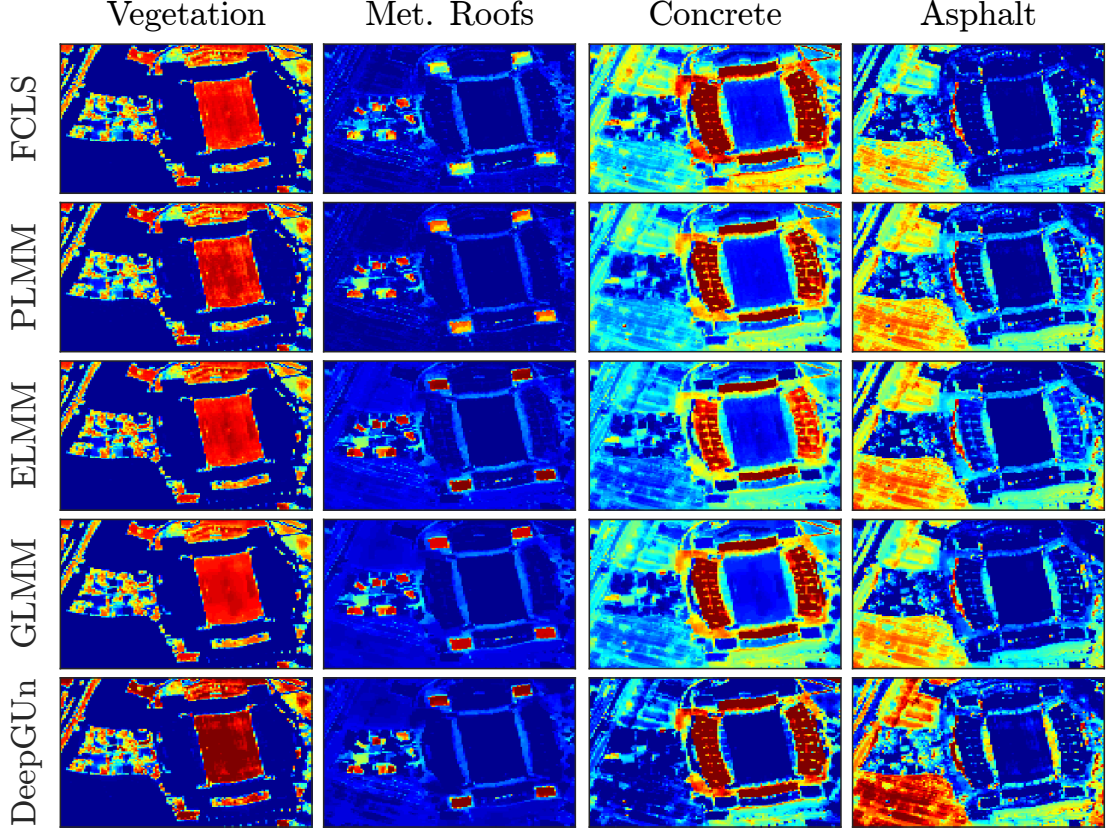


Figure 3: Abundance maps of the Houston dataset for all tested algorithms. Abundance values represented by colors ranging from blue ($\alpha_k = 0$) to red ($\alpha_k = 1$).

Table IV: Simulation results using real data.

	Houston Data		Cuprite Data	
	MSE _Y	Time [s]	MSE _Y	Time [s]
FCLS	0.0478	2.56	0.0057	20.1
PLMM	0.0359	663.25	0.0089	6464.92
ELMM	0.0033	38.3	0.0060	772.75
GLMM	0.0003	48.53	0.0085	4128.49
DeepGUUn	0.0455	259.61	0.0115	7096.73

and low SNR regions were removed, resulting in 188 bands. Previous studies indicate that the Houston HI has four predominant EMs [10], while at least 14 EMs are present at the Cuprite mining field [54].

The reconstructed abundance maps for both datasets and all algorithms are shown in Figs. 3 and 4. For the Houston dataset, the last row of Fig. 3 shows that the abundance maps provided by the DeepGUUn method better evidence the strong vegetation and concrete abundances at the stadium field and stands, respectively, as well as the stronger asphalt abundances in the parking lot. For the Cuprite HI, four EMs were selected whose distribution could be clearly distinguished in the scene [54]. Those EMs are the same already used in [10], [56], [57]. The abundance maps generated by DeepGUUn are shown in the last row of Fig. 4. A careful analysis of these maps shows smooth abundance variations with strong components in the regions of the scene where these materials are known to be present.

The reconstruction errors and execution times for both datasets are shown in Table IV. As was the case for the synthetic data, the DeepGUUn results are worse than those yielded by other methods that address spectral variability. This happens due to its reduced number of degrees of freedom. Nevertheless, we recall that a smaller RMSE_Y does not directly correlate with better abundance reconstructions, the main objective of SU. The execution times of the proposed DeepGUUn method were again comparable to those of the other algorithms addressing spectral variability, which indicates that it scales well with larger image sizes.

VIII. CONCLUSIONS

In this paper, a deep generative EM model was proposed to address spectral variability in SU of HIs. Instead of relying on user-defined parametric EM models which have shown to be very hard to estimate in practical scenes, the proposed methodology leveraged the generalization capability of deep neural networks to accurately model EM spectra while still maintaining a strong connection to the physical mixing process. A deep generative model for each EM was trained prior to unmixing by using pure pixel information extracted directly from the observed HI, which allowed for an unsupervised formulation. The proposed EM model was then applied to solve the SU problem, which was cast as the estimation of the low-dimensional representations of the EMs in the latent space of the deep generative models and their corresponding

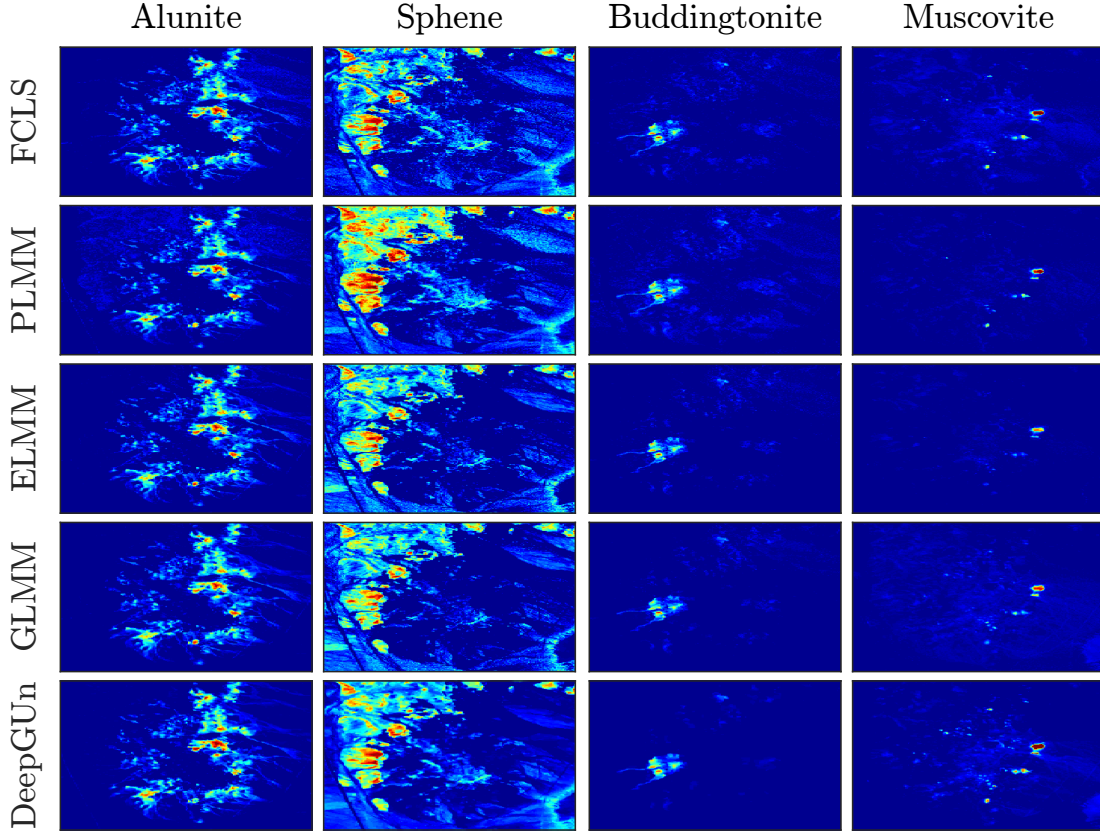


Figure 4: Abundance maps of the Cuprite dataset for all tested algorithms. Abundance values represented by colors ranging from blue ($\alpha_k = 0$) to red ($\alpha_k = 1$).

fractional abundances, for each pixel. The resulting DeepGUUn algorithm presented excellent performance despite the simple strategy used for selecting the training data for learning the generative model. Simulations using synthetic and real data indicate that the proposed method can lead to significant improvements in abundance estimation accuracy.

REFERENCES

- [1] T. Kouyama, Y. Yokota, Y. Ishihara, R. Nakamura, S. Yamamoto, and T. Matsunaga, “Development of an application scheme for the selene/sp lunar reflectance model for radiometric calibration of hyperspectral and multispectral sensors,” *Planetary and Space Science*, vol. 124, pp. 76–83, 2016.
- [2] J. M. Bioucas-Dias, A. Plaza, G. Camps-Valls, P. Scheunders, N. Nasrabadi, and J. Chanussot, “Hyperspectral remote sensing data analysis and future challenges,” *IEEE Geoscience and Remote Sensing Magazine*, vol. 1, no. 2, pp. 6–36, 2013.
- [3] G. Lu and B. Fei, “Medical hyperspectral imaging: a review,” *Journal of biomedical optics*, vol. 19, no. 1, pp. 010901–010901, 2014.
- [4] N. Keshava and J. F. Mustard, “Spectral unmixing,” *IEEE Signal Processing Magazine*, vol. 19, no. 1, pp. 44–57, 2002.
- [5] N. Dobigeon, J.-Y. Tourneret, C. Richard, J. C. M. Bermudez, S. McLaughlin, and A. O. Hero, “Nonlinear unmixing of hyperspectral images: Models and algorithms,” *IEEE Signal Processing Magazine*, vol. 31, no. 1, pp. 82–94, Jan 2014.
- [6] T. Imbiriba, J. C. M. Bermudez, C. Richard, and J.-Y. Tourneret, “Nonparametric detection of nonlinearly mixed pixels and endmember estimation in hyperspectral images,” *IEEE Transactions on Image Processing*, vol. 25, no. 3, pp. 1136–1151, March 2016.
- [7] T. Imbiriba, J. C. M. Bermudez, and C. Richard, “Band selection for nonlinear unmixing of hyperspectral images as a maximal clique problem,” *IEEE Transactions on Image Processing*, vol. 26, no. 5, pp. 2179–2191, May 2017.
- [8] T. Imbiriba, J. C. M. Bermudez, J.-Y. Tourneret, and C. Richard, “Detection of nonlinear mixtures using gaussian processes: Application to hyperspectral imaging,” in *ICASSP, IEEE International Conference on Acoustics, Speech and Signal Processing*, Jan 2014, pp. 7949–7953.
- [9] P.-A. Thouvenin, N. Dobigeon, and J.-Y. Tourneret, “Hyperspectral unmixing with spectral variability using a perturbed linear mixing model,” *IEEE Trans. Signal Processing*, vol. 64, no. 2, pp. 525–538, Feb. 2016.
- [10] L. Drumetz, M.-A. Veganzones, S. Henrot, R. Phlypo, J. Chanussot, and C. Jutten, “Blind hyperspectral unmixing using an extended linear mixing model to address spectral variability,” *IEEE Transactions on Image Processing*, vol. 25, no. 8, pp. 3890–3905, 2016.
- [11] T. Imbiriba, R. A. Borsoi, and J. C. M. Bermudez, “Generalized linear mixing model accounting for endmember variability,” in *Acoustics, Speech and Signal Processing (ICASSP), 2018 IEEE International Conference on*. IEEE, 2018, pp. 1862–1866.
- [12] A. Zare and K. C. Ho, “Endmember variability in hyperspectral analysis: Addressing spectral variability during spectral unmixing,” *Signal Processing Magazine, IEEE*, vol. 31, pp. 95–104, January 2014.
- [13] L. Drumetz, J. Chanussot, and C. Jutten, “Variability of the endmembers in spectral unmixing: recent advances,” in *8th IEEE Workshop on Hyperspectral Image and Signal Processing: Evolution in Remote Sensing*, Los Angeles, USA, 2016.
- [14] R. A. Borsoi, T. Imbiriba, and J. C. Moreira Bermudez, “A Data Dependent Multiscale Model for Hyperspectral Unmixing With Spectral Variability,” *ArXiv e-prints*, Aug. 2018.
- [15] ———, “Super-Resolution for Hyperspectral and Multispectral Image Fusion Accounting for Seasonal Spectral Variability,” *ArXiv e-prints*, Aug. 2018.
- [16] T. Imbiriba, R. A. Borsoi, and J. C. M. Bermudez, “Low-rank tensor modeling for hyperspectral unmixing accounting for spectral variability,” *arXiv preprint arXiv:1811.02413*, 2018.
- [17] R. A. Borsoi, T. Imbiriba, and J. C. M. Bermudez, “Improved hyperspectral unmixing with endmember variability parametrized using an interpolated scaling tensor,” in *2019 IEEE International Conference on Acoustics, Speech and Signal Processing (ICASSP) (submitted)*, 2019.

[18] B. Hapke, "Bidirectional reflectance spectroscopy, 1, Theory," *Journal of Geophysical Research*, vol. 86, no. B4, pp. 3039–3054, 1981.

[19] S. Jacquemoud and S. L. Ustin, "Leaf optical properties: A state of the art," in *8th International Symposium of Physical Measurements & Signatures in Remote Sensing*. CNES, Aussois France, 2001, pp. 223–332.

[20] D. B. Lobell and G. P. Asner, "Moisture effects on soil reflectance," *Soil Science Society of America Journal*, vol. 66, no. 3, pp. 722–727, 2002.

[21] A. Okujeni, S. van der Linden, L. Tits, B. Somers, and P. Hostert, "Support vector regression and synthetically mixed training data for quantifying urban land cover," *Remote Sensing of Environment*, vol. 137, pp. 184–197, 2013.

[22] L. Wang, D. Liu, Q. Wang, and Y. Wang, "Spectral unmixing model based on least squares support vector machine with unmixing residue constraints," *IEEE Geoscience and Remote Sensing Letters*, vol. 10, no. 6, pp. 1592–1596, 2013.

[23] F. A. Mianji and Y. Zhang, "SVM-based unmixing-to-classification conversion for hyperspectral abundance quantification," *IEEE Transactions on Geoscience and Remote Sensing*, vol. 49, no. 11, pp. 4318–4327, 2011.

[24] M. Parente, I. Gemp, and I. Durugkar, "Unmixing in the presence of nuisances with deep generative models," in *Geoscience and Remote Sensing Symposium (IGARSS), 2017 IEEE International*. IEEE, 2017, pp. 5189–5192.

[25] L. Wang and X. Jia, "Integration of soft and hard classifications using extended support vector machines," *IEEE Geoscience and Remote Sensing Letters*, vol. 6, no. 3, pp. 543–547, 2009.

[26] Y. Gu, S. Wang, and X. Jia, "Spectral unmixing in multiple-kernel hilbert space for hyperspectral imagery," *IEEE Transactions on Geoscience and Remote Sensing*, vol. 51, no. 7, pp. 3968–3981, 2013.

[27] X. Li, X. Jia, L. Wang, and K. Zhao, "On spectral unmixing resolution using extended support vector machines," *IEEE Transactions on Geoscience and Remote Sensing*, vol. 53, no. 9, pp. 4985–4996, 2015.

[28] L. Van Der Maaten, E. Postma, and J. Van den Herik, "Dimensionality reduction: A comparative review," *Journal of Machine Learning Research*, vol. 10, pp. 1–41, 2009.

[29] B. Palsson, J. Sigurdsson, J. R. Steinsson, and M. O. Ulfarsson, "Hyperspectral unmixing using a neural network autoencoder," *IEEE Access*, vol. 6, pp. 25 646–25 656, 2018.

[30] R. Guo, W. Wang, and H. Qi, "Hyperspectral image unmixing using autoencoder cascade," in *2015 7th Workshop on Hyperspectral Image and Signal Processing: Evolution in Remote Sensing (WHISPERS)*. IEEE, 2015, pp. 1–4.

[31] Y. Su, A. Marinoni, J. Li, J. Plaza, and P. Gamba, "Stacked nonnegative sparse autoencoders for robust hyperspectral unmixing," *IEEE Geoscience and Remote Sensing Letters*, vol. 15, no. 9, pp. 1427–1431, 2018.

[32] Y. Qu and H. Qi, "uDAS: An untied denoising autoencoder with sparsity for spectral unmixing," *IEEE Transactions on Geoscience and Remote Sensing*, 2018.

[33] S. Ozkan, B. Kaya, and G. B. Akar, "Endnet: Sparse autoencoder network for endmember extraction and hyperspectral unmixing," *IEEE Transactions on Geoscience and Remote Sensing*, no. 99, pp. 1–15, 2018.

[34] Y. Su, J. Li, A. Plaza, A. Marinoni, P. Gamba, and S. Chakravortty, "DAEN: Deep autoencoder networks for hyperspectral unmixing," *IEEE Transactions on Geoscience and Remote Sensing*, 2019.

[35] D. P. Kingma and M. Welling, "Auto-encoding variational bayes," in *Proceedings of the International Conference on Learning Representations (ICLR)*, 2014.

[36] I. Goodfellow, J. Pouget-Abadie, M. Mirza, B. Xu, D. Warde-Farley, S. Ozair, A. Courville, and Y. Bengio, "Generative adversarial nets," in *Advances in neural information processing systems*, 2014, pp. 2672–2680.

[37] R. M. Neal, "Annealed importance sampling," *Statistics and computing*, vol. 11, no. 2, pp. 125–139, 2001.

[38] M. Arjovsky, S. Chintala, and L. Bottou, "Wasserstein generative adversarial networks," in *International Conference on Machine Learning*, 2017, pp. 214–223.

[39] C. Doersch, "Tutorial on variational autoencoders," *arXiv preprint arXiv:1606.05908*, 2016.

[40] V. Shah and C. Hegde, "Solving linear inverse problems using GAN priors: An algorithm with provable guarantees," in *Proc. IEEE Int. Conf. Acoust., Speech, and Signal Processing (ICASSP)*, 2018.

[41] A. Bora, A. Jalal, E. Price, and A. Dimakis, "Compressed sensing using generative models," in *Proc. Int. Conf. Machine Learning*, 2017.

[42] R. Anirudh, J. J. Thiagarajan, B. Kailkhura, and T. Bremer, "An unsupervised approach to solving inverse problems using generative adversarial networks," *arXiv preprint arXiv:1805.07281*, 2018.

[43] M. Asim, F. Shamshad, and A. Ahmed, "Solving bilinear inverse problems using deep generative priors," *arXiv preprint arXiv:1802.04073*, 2018.

[44] M.-D. Iordache, J. M. Bioucas-Dias, and A. Plaza, "Sparse unmixing of hyperspectral data," *IEEE Transactions on Geoscience and Remote Sensing*, vol. 49, no. 6, pp. 2014–2039, 2011.

[45] B. Somers, M. Zortea, A. Plaza, and G. P. Asner, "Automated extraction of image-based endmember bundles for improved spectral unmixing," *IEEE Journal of Selected Topics in Applied Earth Observations and Remote Sensing*, vol. 5, no. 2, pp. 396–408, 2012.

[46] B. Somers, L. Tits, D. Roberts, and E. Wetherley, "Endmember library approaches to resolve spectral mixing problems in remotely sensed data: Potential, challenges, and applications," in *Data Handling in Science and Technology*. Elsevier, 2016, vol. 30, pp. 551–577.

[47] J. Nocedal and S. Wright, *Numerical Optimization*. Springer Science & Business Media, 2006.

[48] P. Hand and V. Voroninski, "Global guarantees for enforcing deep generative priors by empirical risk," in *Proceedings of the 31st Conference On Learning Theory*, ser. Proceedings of Machine Learning Research, S. Bubeck, V. Perchet, and P. Rigollet, Eds., vol. 75. PMLR, 06–09 Jul 2018, pp. 970–978.

[49] A. S. Lewis and M. L. Overton, "Nonsmooth optimization via quasi-newton methods," *Mathematical Programming*, vol. 141, no. 1-2, pp. 135–163, 2013.

[50] F. E. Curtis and X. Que, "A quasi-newton algorithm for nonconvex, non-smooth optimization with global convergence guarantees," *Mathematical Programming Computation*, vol. 7, no. 4, pp. 399–428, 2015.

[51] S. Boyd, N. Parikh, E. Chu, B. Peleato, and J. Eckstein, "Distributed optimization and statistical learning via the alternating direction method of multipliers," *Found. Trends Mach. Learn.*, vol. 3, no. 1, pp. 1–122, Jan. 2011.

[52] L. Van der Maaten, "Matlab toolbox for dimensionality reduction." [Online]. Available: <https://vdmaaten.github.io/drtoolbox/code/drtoolbox.tar.gz>

[53] D. P. Kingma and J. Ba, "Adam: A method for stochastic optimization," in *International Conference on Learning Representation*, 2015.

[54] J. M. P. Nascimento and J. M. Bioucas-Dias, "Vertex Component Analysis: A fast algorithm to unmix hyperspectral data," *IEEE Transactions on Geoscience and Remote Sensing*, vol. 43, no. 4, pp. 898–910, April 2005.

[55] R. N. Clark, G. A. Swayze, K. E. Livo, R. F. Kokaly, S. J. Sutley, J. B. Dalton, R. R. McDougal, and C. A. Gent, "Imaging spectroscopy: Earth and planetary remote sensing with the USGS tetracorder and expert systems," *Journal of Geophysical Research: Planets*, vol. 108, no. E12, 2003.

[56] R. A. Borsoi, T. Imbiriba, J. C. Moreira Bermudez, and C. Richard, "A Fast Multiscale Spatial Regularization for Sparse Hyperspectral Unmixing," *IEEE Geoscience and Remote Sensing Letters*, 2018.

[57] T. Imbiriba, R. A. Borsoi, and J. C. M. Bermudez, "A low-rank tensor regularization strategy for hyperspectral unmixing," in *2018 IEEE Statistical Signal Processing Workshop (SSP)*, 2018, pp. 373–377.